Theoretical and Experimental Studies of the Reactions between Hyperthermal O(^{3}P) and Graphite: Graphene-Based Direct Dynamics and Beam-Surface Scattering Approaches†

Jeffrey T. Paci,*,‡ Hari P. Upadhyaya,§ Jianming Zhang,§ George C. Schatz,|| and Timothy K. Minton§

Department of Chemistry, University of Victoria, P.O. Box 3065, Victoria, British Columbia, Canada V8W 3V6, Department of Chemistry and Biochemistry, Montana State University, Bozeman, Montana 59717, and Department of Chemistry, Northwestern University, 2145 Sheridan Road, Evanston, Illinois 60208-3113

Received: January 3, 2009; Revised Manuscript Received: February 17, 2009

Beam-surface scattering experiments and theoretical direct dynamics based on density functional theory calculations are used to investigate hyperthermal collisions between O(^{3}P) and highly oriented pyrolytic graphite (HOPG). The simulations suggest that the HOPG surface becomes functionalized with epoxide groups. Intersystem crossing (ISC) between the lowest-energy triplet and singlet potential-energy surfaces is not necessary for this functionalization to occur. Both theory and experiment indicate that incoming O atoms can react at the surface to form O_2 by way of an Eley−Rideal mechanism. They also suggest that the collisions can result in the production of CO and CO_2 by way of both direct and complex reaction mechanisms. The direct dynamics simulations provide significant insight into the details of the complex reaction mechanisms. Semiquinones are present at defect sites and can form in functionalized pristine sheets, the latter resulting in the formation of a defect. Direct collision of an incoming O atom with a semiquinone or vibrational excitation caused by a nearby O-atom collision can cause the release of the semiquinone CO, forming carbon monoxide. The CO may react with an oxygen atom on the surface to become CO_2 before receding from the surface. The simulations also illustrate how epoxide groups neighboring semiquinones catalyze the release of CO. Throughout, the experimental results are observed to be consistent with the theoretical calculations.

I. Introduction

Organic thin films, polymers, and carbon fiber reinforced composites, which are now commonly used in spacecraft applications, are exposed to atomic oxygen [O(^{3}P)] in low-Earth orbit (LEO). Because of their high relative velocity, collisions between these oxygen atoms and spacecraft occur with energies of more than 5 eV. It is important to characterize the damage these violent collisions cause if these materials are to be improved. With this as motivation, highly oriented pyrolytic graphite (HOPG) has frequently been used to investigate the behavior of carbon-based materials in these kinds of environments.[1−4]

Hydrocarbon-based fuels are frequently used as rocket propellants. Soot, which is largely composed of small particles of graphite and amorphous carbon, is present in the exhaust.[5−8] Collisions between these particles and O(^{3}P) occur at hyperthermal energies because of the high velocity of the rocket exhaust relative to the ambient O atoms present in LEO. Therefore, a fuller understanding of the reactions that occur between graphite and hyperthermal O atoms is also of significant interest to the rocket plume research community.

Experiments done to date on the effects of hyperthermal atomic oxygen on HOPG have focused on postexposure characterization of HOPG surfaces. Tagawa and coworkers[1] studied the morphology and chemical composition of an HOPG surface after it was exposed, at room temperature, to atomic oxygen. They found that oxygen coverage reached a saturation level with atomic-oxygen fluences greater than 4×10^{17} atoms per cm^2. Analysis of the C 1s peak by X-ray photoelectron spectroscopy revealed the presence of C−O, C═O, or O−C−O, and O−C═O. Scanning tunneling microscopy showed that the HOPG surface became rough and formed hillock-like structures. Nicholson, Minton, and Sibener[2−4] conducted a series of experiments to study the chemical reactivity and morphological evolution of HOPG upon exposure to 5 eV O atoms, and they found a strong dependence of reactivity on surface temperature. The reaction rate almost tripled from 298 to 493 K. At 298 K, the resulting surface morphology was rough on an atomic scale, and the entire surface was decorated with circular etch pits whose diameters spanned nanometers to microns and whose depths ranged from a few nanometers to tens of nanometers, depending on the O-atom fluence. When the sample temperature was increased to 493 K, the resulting surface morphology exhibited no circular pits but instead large towers and hillocks spanning hundreds of nanometers. These effects were discussed in terms of an anisotropic reactivity of hyperthermal atomic oxygen with prismatic and basal carbon sites. However, the detailed reaction mechanisms were not elucidated. Note that in the above experiments, the O atoms were accompanied by O_2 molecules that had the same velocity as the O atoms. Therefore, O_2 had twice the translational energy of O. The role of O_2 in the reaction of the hyperthermal beam with HOPG is not clear.

HOPG is composed of crystallites that have their *c* axis parallel to the surface normal of the crystal and which are several microns to several tens of microns in size along the basal planes.[1,9] It has a point defect density inside the crystallites that may be as low as 3 to 4 μm^{-2}.[1] In many of the experiments, there were significant concentrations of both O(^{3}P) and O_2 in

† Part of the special issue "George C. Schatz Festschrift".

* Corresponding author. E-mail: jtpaci@uvic.ca.
‡ University of Victoria.
§ Montana State University.
|| Northwestern University.

10.1021/jp9000412 CCC: $40.75
Published on Web 03/20/2009

the incident beam, so these point defects should be quickly functionalized by the colliding O and O_2, resulting in the formation of a variety of functional groups.[10,11] The barrier to O_2 dissociative chemisorption at HOPG defects sites is low,[10,12,13] and O(^{3}P) will readily bind in a barrierless process. The HOPG, if exposed to air after cleavage, may have a significant number of oxygen molecules associated with its surface even before it is exposed to a hyperthermal beam source.[9]

Once exposed in a beam experiment, the graphite surface will become functionalized with epoxide groups that can migrate across the surface, spending some of their time as atop oxygen atoms as they move (atop oxygen: an oxygen atom (oxy radical) bonded to a single carbon atom, with the resulting C−O bond being perpendicular to the graphite basal plane).[1,14] O_2 can physisorb, although it is only bound to a pristine surface by a small barrier (∼0.1 eV),[15−17] so most O_2 is expected to scatter inelastically from the surface. Thermal O_2 may physisorb. At a temperature of ∼500 K, close to the temperature used in many of the experiments, O_2 molecules can also move around the surface.[14,18,19] Only oxygen atoms chemically bonded at defect sites are likely to be immobile, except for the possibility of leaving the surface as part of an O_2, CO, CO_2, or other small molecule.

The surface of the HOPG is eroded by a beam containing 5 eV oxygen atoms.[1−4] Neither 5 eV oxygen atoms nor 10 eV oxygen molecules are expected to cause sputtering from a pristine unfunctionalized surface.[1,20] However, they may cause the removal of small molecules from defect sites or from pristine sites, which are already populated with atop and epoxide oxygen atoms. In the case of the pristine sites, new defect sites would then be formed.

The density of preexisting defects alone is not sufficiently high to explain the experimental observations.[1−4] Additional defects must be formed, which then act as nucleation sites for further etching. As mentioned, collisions with functional groups already on the surface is one possible route to the creation of new defects. However, we have also observed the spontaneous formation of holes in defect-free graphene sheets in our molecular dynamics (MD) simulations of graphite oxide (GO).[14] The chemistry that occurs in our models of GO is somewhat different than that expected in our O + graphite models largely because of the presence of a significant concentration of hydroxyl groups in addition to epoxide groups on the surface of the former. However, GO chemistry is dominated by epoxide groups, which, as will become clear below, is also the case in O + graphite. This suggests that the spontaneous formation of holes may also be possible in the O + graphite system.

Many of the reactions observed in both of these systems are also closely related to those that occur in combustion and gasification chemistry. Previous studies suggest that the rate-limiting step during the gasification of graphite is associated with a barrier height of ∼40 kcal/mol (1.7 eV)[21−24] and involves a reaction that at least initially produces CO.[25,26] (The CO may go on to become CO_2.) This is the size of the threshold for CO production that is expected to be important in this work. There is yet to be a consensus on exactly which reaction is associated with this barrier. However, there is strong evidence of it being associated with a rearrangement that involves the movement of epoxide groups toward sheet edges or defects sites that are functionalized by semiquinones;[11,12] the semiquinones dissociate to produce a CO, and the epoxide groups move to form new C═O functional groups (semiquinones or carbonyls). There is also evidence that epoxide groups neighboring semiquinones weaken carbon−carbon bonds and facilitate the dissociation of the CO.[11,12] Dioxiranes are also of interest because their formation can provide a direct source of CO_2 (CO_2 produced without first producing CO).[22] It has been shown that the process is associated with a relatively low reaction barrier.[13]

At ∼500 K, it is expected that some CO will leave the HOPG surface spontaneously and thus be a source of thermal CO. Once it has left the surface, the CO may go on to react with other oxygen atoms on the surface to form CO_2. The carbon atom that departs the surface will leave behind one or more atoms with unsatisfied valencies (dangling bonds). Oxygen atoms that are on the surface in the form of epoxides and atop oxygens can migrate to these atoms and bond. Physisorbed O_2 can also move and react at these sites. New C═O groups are thus formed, which can also leave the surface spontaneously or after collision with additional incoming oxygen atoms or molecules.

Oxygen-containing groups at defect sites will be struck by incoming hyperthermal oxygen atoms, which may cause the release of CO/CO_2. Hyperthermal oxygen atoms may also collide with dangling-bond carbons and cause the release of CO. However, the relatively low flux of oxygen atoms and molecules in the beam and relatively high rate of oxygen atom and molecule migration on the surface make the latter unlikely.

Some theoretical work aimed at investigating the processes just described has already been performed and involved various types of trajectory studies.[20,27−29] One is particularly relevant to the present work. In it, the loss function for graphite subject to oxygen collisions was estimated using classical trajectories.[20] This work suggested that the erosion process takes place in two steps. The first involves the functionalization of the surface by an oxygen collision (epoxide formation), and the second involves the removal of this group as CO, resulting from a subsequent oxygen-atom collision. The work suggests that it is the former that is the rate-limiting step and that epoxide formation requires intersystem crossing (ISC) between the lowest-lying triplet and singlet potential-energy surfaces. The model used in this study was based on ethylene−oxygen potentials, which may have limited the accuracy of resulting dynamical predictions. It also did not provide a description of what might occur when an incoming oxygen atom encounters a functional group at a defect site or encounters more than one functional group on the surface.

Running quasi-classical trajectories based on direct dynamics provides a way to obtain additional insight into aspects of the O(^{3}P) + graphite system. This is the approach we adopted for the present work. We examined the collision processes by modeling graphite using a single layer (graphene) with periodic boundary conditions (PBCs). On this layer, functional groups were placed in random locations, with the intention of elucidating the reactions that might take place during and subsequent to the collision of a hyperthermal oxygen atom with an oxygen-functionalized graphite surface. The role played by vacancy defects, semiquinones, dioxiranes, epoxides, atop oxygen atoms, and other functional groups was explored. The calculations are augmented by molecular beam-surface scattering experiments in which the products O, O_2, CO, and CO_2 were monitored. The experimental results are consistent with the theoretical calculations.

II. Experimental Methods

The experiments were performed with the use of a crossed molecular beams apparatus,[30−32] which was coupled to a laser-breakdown hyperthermal beam source[33] and configured for beam-surface scattering experiments. In brief, a pulsed beam containing hyperthermal O and O_2 was directed at a resistively

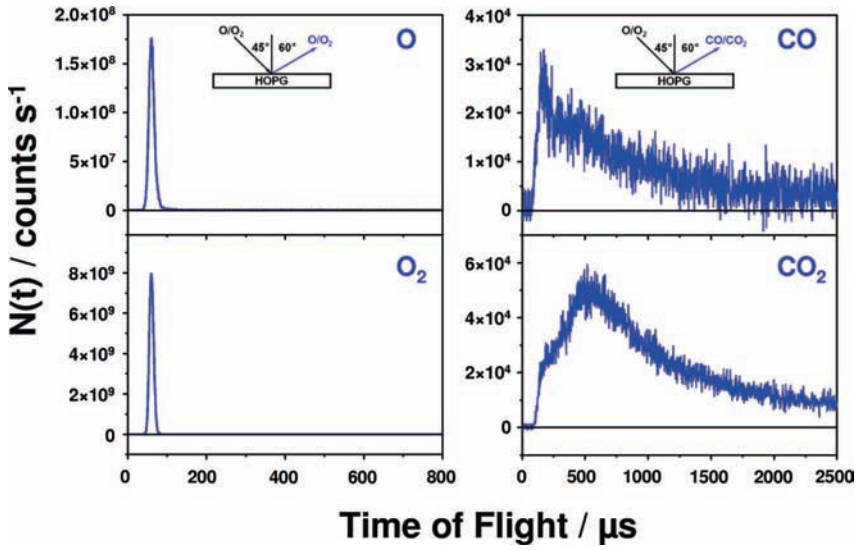

Figure 1. Representative time-of-flight distributions of O, O_2, CO, and CO_2 that scatter from an HOPG surface, held at 503 K, following impingement of the hyperthermal O/O_2 pulse at an incident angle, θ_i, of 45°. In the example shown, the products were detected at a final angle, θ_f, of 60°.

heated HOPG surface, and a rotatable mass spectrometer detector was used to monitor the products that scattered from the surface. The surface and detector rotate about the same axis, with the surface normal rotating in the same plane as the detector. To characterize the hyperthermal beam, the surface was lowered out of the beam path, and the beam was directed into the detector. Measurements of the beam were used to determine the translational energy distributions of the components of the beam and their relative fluxes.

The pulsed hyperthermal beam, which operated at a repetition rate of 2 Hz, contained atomic and molecular oxygen. A synchronized chopper wheel was used to select a narrow portion of the hyperthermal beam pulse. The average translational energy of the O atoms in the beam was 503 kJ·mol^{-1} with an energy width (fwhm) of 65 kJ·mol^{-1}. The molecular oxygen in the beam had an average translational energy of 1006 kJ·mol^{-1} and width of 130 kJ·mol^{-1}. The fraction of atomic oxygen was about 68%, and the atomic oxygen was in its ground electronic state, O(^{3}P).[34] The molecular oxygen was also in its ground state, O_2 ($^3\Sigma_g^-$).[35]

We prepared the HOPG samples (ZYA quality, Advanced Ceramics) by cleaving the sample in air with tape and immediately placing the sample into the vacuum chamber. The base pressure of the main scattering chamber was 1×10^{-7} torr, and the operation pressure was less than 2×10^{-7} torr. The sample was first heated under vacuum at 540 K for ~60 h to remove contamination and anneal the surface. The sample temperature was then reduced to 503 K for data collection. This high temperature ensured that the sample was free from contamination.[36]

Number density distributions of products that scattered from the surface were collected as a function of their arrival time in the electron impact ionizer of the detector, which was 33.7 cm from the surface. These distributions, referred to as time-of-flight (TOF) distributions, were collected at an incident angle, θ_i, of 45° and a variety of final angles, θ_f. For each θ_f, TOF distributions at m/z = 16 (O^+), 32 (O_2^+), 28 (CO^+), and 44 (CO_2^+) were accumulated for a total of 400, 400, 3000, and 1500 beam pulses, respectively. These data were collected under steady-state conditions.

III. Experimental Results

Representative TOF distributions for O, O_2, CO, and CO_2 are presented in Figure 1. These distributions were collected with $\theta_i = 45°$ and $\theta_f = 60°$. Time zero in the TOF distributions corresponds to the nominal time at which the hyperthermal O/O_2 pulse struck the surface. The scattered O and O_2 have very narrow TOF distributions and similar flight times. The peaks at about 60 μs indicate hyperthermal scattering with final translational energies of about half the respective incident energies. If O or O_2 had scattered from the surface with translational energies dictated by the surface temperature (thermal scattering), then their flight times would have been ~500−600 μs. As seen in the TOF distributions for O and O_2, only hyperthermal scattering is observed. However, the TOF distributions of CO and CO_2 are obviously bimodal. The peak (or shoulder) at ~200 μs corresponds to hyperthermal scattering and the peak at ~500 μs corresponds to thermal scattering. The hyperthermal components indicate products formed on a time scale that is too short for thermal equilibrium with the surface to be reached. The thermal components (longer arrival times) indicate products released from the surface after thermal equilibrium has been attained. The thermal components of CO and CO_2 TOF distributions have very long tails that extend beyond 4000 μs (not shown in the Figure). Apparently, some CO and CO_2 may not form promptly after the hyperthermal O/O_2 beam strikes the surface, or these products may have a long residence time on the surface before desorbing. The relative intensities of the hyperthermal and thermal components of the CO and CO_2 TOF distributions were determined in a manner that has been previously described.[31]

Figure 2a shows the angular distribution of scattered O and O_2 flux with $\theta_i = 45°$. The relative intensities have been corrected for the difference in ionization cross section between O and O_2. Both O and O_2 peak sharply at a final (superspecular) angle of 60°. Similar angular dependence has also been observed for inelastic scattering of hyperthermal Ar from an HOPG surface.[36] In the vicinity of the sharp peak, the scattered O_2 flux is much higher than that of O. (Note the two different scales.) As seen in Figure 2b, the ratio of O_2 to O flux mirrors the angular distributions of these products and rises to a maximum of about 20 at a θ_f near 60°. Given that the O_2/O flux ratio in the beam is ~0.48, the results in Figure 2 clearly indicate the significant production of O_2 at the surface. The observation of only hyperthermal O_2 (Figure 1) that is scattered in the superspecular direction suggests that incident O atoms react

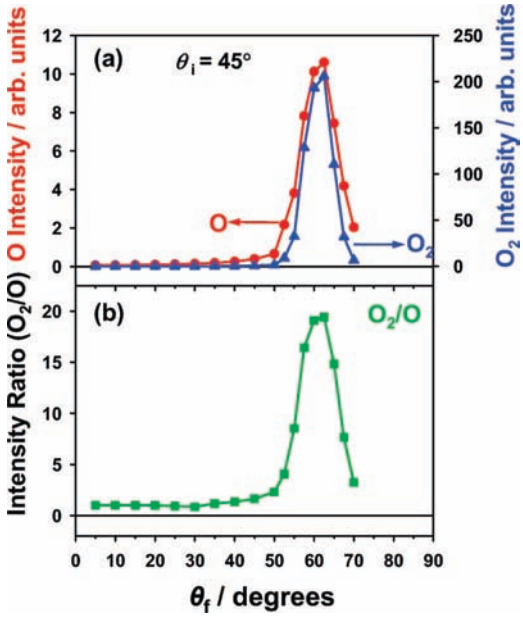

Figure 2. (a) Relative flux of scattered O (red circles, left vertical axis) and O_2 (blue triangles, right vertical axis) as a function of θ_f, with $\theta_i = 45°$. (b) Ratio of O_2 flux to O flux as a function of θ_f.

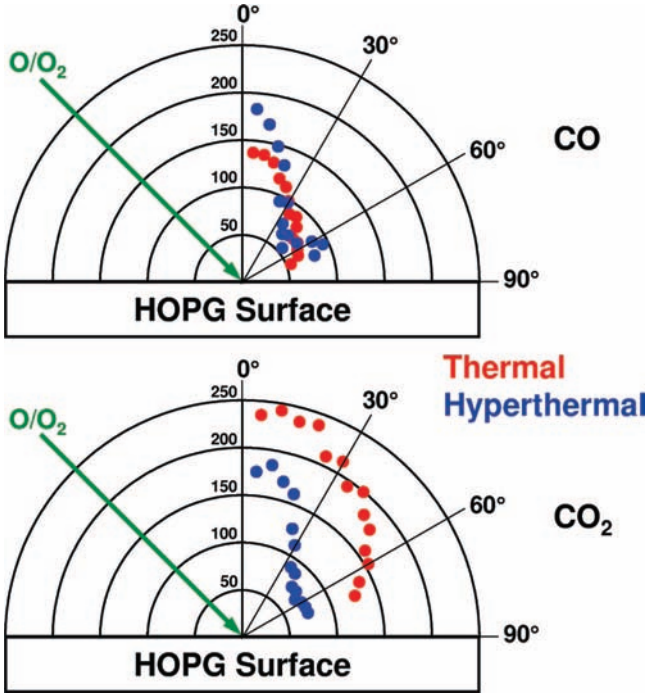

Figure 3. Relative flux of scattered CO (top panel) and CO_2 (bottom panel) as a function of θ_f, with $\theta_i = 45°$. Red circles represent the flux of the thermal components and blue circles represent the flux of the hyperthermal components.

directly with O on the surface to produce O_2 that scatters from the surface in an Eley−Rideal mechanism.

The angular distributions of CO and CO_2 are shown in Figure 3. The intensities of CO and CO_2 are plotted on the same scale and have been corrected for the differences in number of beam pulses, ionization cross section, and dissociative ionization patterns[37−41] so that the relative intensities can be directly compared. For both CO and CO_2, the angular distributions of the thermal components appear to have maxima along the surface normal and decrease with increasing θ_f. The angular distributions of the hyperthermal components also appear to have maxima along the surface normal, and they exhibit secondary maxima near $\theta_f = 60°$. Scattering along the surface normal suggests a complex reaction mechanism on the surface, whereas scattering in the superspecular direction with hyperthermal velocities suggests a direct reaction between the incident species and a surface moiety.

IV. Theoretical Methods

Theoretical investigations of these processes were undertaken. Direct dynamics calculations were performed with forces and energies derived from density functional theory (DFT) calculations. The Spanish initiative for electronic simulations with thousands of atoms (SIESTA) package[42,43] was used to perform the DFT, and the Perdew−Burke−Ernzerhof (PBE)[44] GGA functional with a double-ζ plus polarization (DZP) basis set was employed. The Γ point was used for the Brillouin zone sampling and a diagonalization to solve the Kohn−Sham equations. The models used were based on a 24-atom graphene sheet.

Three-dimensional PBCs were used. The two unit cell vectors within the graphene basal plane were optimized so that the pristine sheet was under zero stress. Their postoptimization magnitudes were 7.46 and 8.66 Å in the x and y directions, respectively. The unit cell vector perpendicular to the basal plane had a magnitude of 30 Å and pointed in the z direction. Testing suggested that this was large enough for there to be no significant interaction been the sheet and its replicas in neighboring unit cells in the z direction. These unit cell vectors were then fixed at these values for all of the simulations.

A pristine sheet and sheets containing a single-atom vacancy defect were studied. As discussed in Section II, it is unlikely that an oxygen atom with a collision energy of 5 eV would result in the removal of one or more carbon atoms from an unfunctionalized pristine graphene sheet. Therefore, we investigated a pristine sheet functionalized with eight oxygen atoms to explore the behavior of sheets without preexisting holes. We also chose to examine a single-atom vacancy because it is one of the next simplest structures that could be considered. Because dangling bonds are unlikely to exist for extended periods of time in an oxygen-rich environment, we capped their valencies with oxygen atoms. Sheets functionalized with two, four, and eight oxygen atoms were investigated. Surface roughness on a scale larger than the unit cell was not considered.

The structure shown in Figure 4a illustrates how the valencies at the single-atom vacancy were satisfied. The structure contains two oxygen atoms and has been frequently observed in our Monte Carlo and MD simulations of GO.[14] It is stable and contains a semiquinone group that is known from combustion chemistry to be important at holes in and at the edges of graphene sheets.[11,12] The structure will be referred to as Model A.

Motivated by the work in refs 11 and 12, we also investigated the structure shown in Figure 4b (Model B). The semiquinone that it contains should have carbon−carbon bonds that are weakened by the neighboring epoxide groups, which increases the probability of it dissociating to form CO or CO_2. Although this intentional arrangement of a structure is not random and thus may bias for CO/CO_2 release in a nonstatistical way, it will later become clear that the migration of epoxides is a highly probable event. Therefore, the formation of such a structure is also highly probable. This nonrandom arrangement was investigated in hope of increasing the probability of observing dissociative events during our short-time simulations, which are restricted in terms of propagation times by our limited (albeit substantial) computational resources.

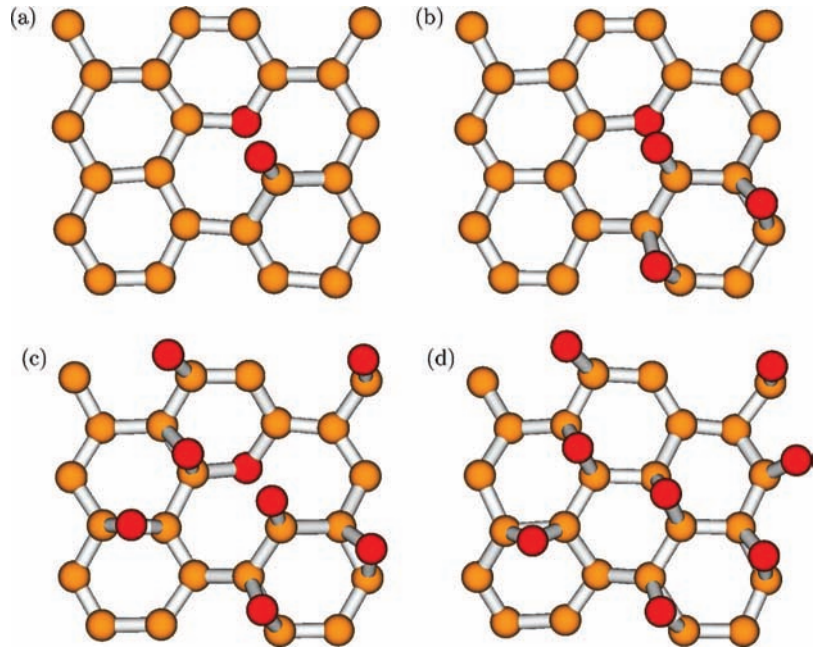

Figure 4. Precollision structures. A graphene sheet containing a single-atom vacancy defect and (a) two oxygen atoms (Model A), (b) four oxygen atoms (Model B), and (c) eight oxygen atoms (Model C). (d) A pristine graphene sheet functionalized with eight oxygen atoms (Model D). Carbon atoms are light yellow and oxygen atoms are dark red.

Additional oxygen atoms were added to the sheet to create the models shown in Figure 4c,d (Models C and D, respectively). Their positions were selected at random from all of the remaining physically realistic sites for atop- and epoxide-oxygen atoms on the surface side of the sheet. The addition of functional groups to the bulk side (side opposite the incoming oxygen atom) of the sheet was not considered because it would not be accessible in the experiments. Note that because of the PBCs, the oxygen atoms in Models C and D at the edges of the sheet that appear to be attached to the sheet by only one bond are in fact attached by two bonds. The carbon atoms to which the second bonds extend can be envisioned by imagining a shift of the graphene lattice by the appropriate unit cell vector within the plane of the page. There are no atop oxygen atoms in Models C or D. Although they were present in the structures before geometry optimization, in all cases, they relaxed to form epoxide groups.

We ran intramolecular trajectories for the O + graphite models before exposing them to a colliding oxygen atom. They were randomly sampled to provide a set of initial conditions for the direct dynamics trajectories. MD simulations at 525 K were used.

Sheets were exposed to oxygen atoms traveling with 5 eV of kinetic energy, approximately matching the collision energies used in the current (503 kJ·mol^{-1} = 5.2 eV) and some of the earlier experiments.[2−4] Normal incidence was considered, with impact locations chosen at random. Each direct dynamics calculation was performed twice, with each set of initial conditions run once in the lowest-energy singlet and once in lowest-energy triplet electronic state. For each of the four models, 100 singlet and 100 triplet trajectories were run, and each was 1 ps in duration. A time step of 40 au (0.97 fs) was used.

A proper accounting for the effect of spin−orbit coupling between these two electronic states would be beneficial.[20,28,45,46] Surface hopping-[20] and Ehrenfest dynamics-based[28] techniques, which approximately account for this nonadiabaticity, have been used to investigate limited aspects of the O + graphite problem. However, using either of these techniques to investigate the reactive events described here is computationally impractical.

PBE/DZP is expected to predict bond lengths and angles to an accuracy of a few tenths of an angstrom and a few degrees, respectively, for the systems studied here. However, the barrier heights associated with the chemical reactions are unlikely to be predicted with the same high level of accuracy.

After the impact, adsorption, or both of the colliding oxygen atom, the O + graphite sheet becomes vibrationally excited. Because the system is not coupled to a thermal bath, this excitation results in an increase in temperature. The collision causes the breaking and creation of new chemical bonds, so it would be difficult to accurately calculate the increase in temperature. Coupling the system to a thermal bath would be unrealistic because localized vibrational excitation is a critical aspect of the dynamics we simulated here. This is because it causes reactions to occur, as the shockwave caused by the incoming oxygen atom moves outward from the location of impact, that would otherwise not occur. It is the confinement of the shockwave by the finite sheet size that causes the heating. These complications limit the propagation time for which the trajectories can be accurately propagated. However, we expect these issues to have only a minor effect on the accuracy of the reported short-time dynamics.

The use of PBE/DZP for this problem was marginally computationally practical. The singlet calculations (spin-unpolarized) for Model A ran at a rate of ∼500 fs/day on a modern Xeon processor. Note that this rate widely varied. In some cases, it was much lower because of variations in the times required for self-consistent field (SCF) convergence. The trajectories proceeded the least quickly when the oxygen atom was relatively far from the surface because SCF convergence was especially time-consuming for these configurations. Whenever possible, we made use of the electron density from the previous time step as a starting guess for the new density. Doing so usually greatly accelerates SCF convergence.

In the two- and four-oxygen atom O + graphite sheet simulations, an initial basal plane to incoming-oxygen-atom

TABLE 1: Some of the Reactions Observed during the Trajectories That Were Run on the Lowest-Energy Singlet Potential-Energy Surface[a]

reaction	model A	model B	model C	model D
ring opening	36	9	9	0
epoxide formation	76	77	33	7
epoxide migration	37	34	11	21
carbonyl formation	3	1	0	0
O_2 formation	1	17	55	79
CO_2 formation	0	1	2	0
CO formation	0	1	6	0
dioxirane formation	0	2	1	0
inelastic O	0	0	1	0
sheet damage	0	0	0	3

[a] For each model, 100 trajectories were propagated. Results for the four models described in Figure 4 are shown. See the text for details beyond the abbreviated descriptions of the reactions provided in the first column. The other reactions that were observed are summarized in an analogous table in the Supporting Information.

TABLE 2: Same As Table 1 except the Results Correspond to Trajectories That Were Run on the Lowest-Energy Triplet Potential-Energy Surface

reaction	model A	model B	model C	model D
ring opening	32	17	16	0
epoxide formation	75	70	29	17
epoxide migration	21	46	20	17
carbonyl formation	2	0	0	0
O_2 formation	0	17	53	76
CO_2 formation	0	3	1	0
dioxirane formation	0	0	1	0
inelastic O	0	7	13	4
sheet damage	0	0	0	2

separation of 10 au (5.3 Å) was used. This distance was reduced to 8 au in the eight oxygen atom and pristine sheet simulations, which partially alleviated SCF-related delays. Testing suggested that using smaller initial separations would have led to unphysical behavior. Although an 8 au incoming oxygen atom to basal plane separation may seem quite large, the O + graphite functional groups protruded from the surface and thus reduced the separation between them and the incoming oxygen atom to, in some cases, well below this distance.

The triplet calculations (spin-polarized with an overall fixed spin of two excess spin-up electrons) ran significantly more slowly than the singlet calculations. There was not only a factor-of-two slowdown associated with having to consider the spin-up and -down electrons separately but also additional convergence issues. These made it necessary to write software to detect problems and, when appropriate, to make multiple attempts at SCF convergence at a given geometry by using different sets of convergence tools. This combination of challenges meant that the triplet calculations ran at a rate of ~100 fs/day when using Model A.

V. Theoretical Results and Discussion

Trajectories for each model resulted in a variety of reactions. Some of the more interesting reactions and the number of times they were observed are summarized in Tables 1 and 2 for the trajectories run on the lowest-energy singlet and lowest-energy triplet potential-energy surfaces, respectively. The other reactions observed are summarized in analogous tables in the Supporting Information. For the most part, aside from the observation of slightly different numbers of singlet versus triplet reactive events, the dynamics and types of reactivity observed in both cases were similar. Because of this and the limited number of interesting reactive events observed, a distinction will usually not be made between singlet and triplet trajectories in the discussion that follows.

As discussed in Section II, incoming oxygen atoms in the experiment were in the ^3P electronic state. Graphite was expected to be in its singlet ground state. It is not entirely clear what happens electronically as the oxygen atoms approach the surface. ISC is not likely to be important during 1 ps hyperthermal collisions, but it could play a role for longer times.[47,48] The fact that the results did not strongly depend on whether the dynamics took place in the singlet or triplet state suggests that if ISC crossing had been included, then it would not have had a dramatic effect.

A more detailed description of some of the reactions summarized in column one of Tables 1 and 2 is warranted. The descriptions for those that are less self-explanatory are (1) Ring opening: The breaking of a C−O bond in the oxygen-containing six-membered ring; (2) Epoxide migration: The movement of an oxygen atom from one epoxide location to another. The oxygen atom moved atop a carbon atom in the process, sometimes lingering there for tens of femtoseconds; (3) Carbonyl formation: A CO group attached to the sheet by one bond to the carbon atom; (4) Inelastic O: The incoming oxygen atom underwent an inelastic collision with the surface and then scattered away; (5) Sheet damage: The breaking of a C−C bond in the pristine sheet. Many of these reactive events cannot be easily observed experimentally because they occur on such small length-scales.

When oxygen was removed from the surface, this usually occurred by way of the formation of O_2. Nearly all reactions that resulted in its formation did so by way of an Eley−Rideal mechanism, which is consistent with the experimental observations. Also consistent with experiment is the fact that the reaction of an incoming O atom with an O atom on the surface to produce O_2 is a highly probable event. (See Figure 2.) Postimpact (Langmuir−Hinshelwood) production of O_2 was also observed but occurred less than 2.4% of the time. The ground electronic state of O_2 is a triplet. As was expected, when O_2 was formed in the triplet (spin-polarized) calculations, it was in a triplet electronic state.

The formation of O_2 by way of an Eley−Rideal-type reaction could be modeled using a simpler computational method. The prompt departure of the products makes the dynamics of the surface unimportant. However, in addition to this reaction, we were interested in modeling the broad range of reactions that might occur subsequent to O-atom impact. Therefore, we developed a more complete theoretical treatment.

The presence of carbonyl groups on our O + graphite sheets suggests a plausible source for the superspecular scattering shown in Figure 3. The barrier to dissociation of these groups is small compared with that associated with the release of CO/CO_2 from a semiquinone.[11] Therefore, the collision of an incoming oxygen atom or molecule with such a group could reasonably be expected to lead to a direct reaction producing CO/CO_2.

Figure 3 also shows that CO and CO_2 have comparable fluxes, which is consistent with the trajectory results. Note that there could be additional mechanisms for CO/CO_2 production in the experiments that were not part of the calculations and that very few trajectories led to CO and CO_2. These few trajectories provided poor statistics for this flux comparison.

For both the singlet and triplet trajectories run using Model A, the incoming oxygen atom became bound to the surface in

every case. This suggests that the concentration of oxygen atoms in this model is significantly below the nearly steady-state concentration that would have been established during prolonged exposure to the oxygen beam in the experiments. It is probable that Model B also has an oxygen-atom coverage below this concentration because incoming oxygen atoms have a higher probability of binding than they have of removing another oxygen atom from the sheet. When Model C was used, more than half of the trajectories resulted in the production of O_2 for both types of trajectories. This suggests that the concentration of oxygen atoms in this model was higher than the experimental surface concentration. Combined, these results suggest that the steady-state oxygen coverage in the experiments is in between the concentrations used in Models B and C.

In contrast with the work of Cohen,[20] the relatively high probability for epoxide formation, and relatively low probability of CO/CO_2 production suggests that the latter is the rate-limiting step in the erosion process. Epoxide groups form in both the singlet and triplet trajectories, which is consistent with our earlier work on O + ethylene, where epoxides were observed to form on the triplet state.[48] This suggests that ISC is only of secondary importance.

It is unclear what impact the excess oxygen concentration in Models C and D had on the dynamics. Observations suggest that higher levels of functionalization lead to a larger probability of producing CO and CO_2. This is presumably because clusters of functional groups lower the threshold for CO and CO_2 release. Similar clusters suitable for catalyzing the various reactions are also likely to exist at various times during the experiments. An excess of oxygen may simply make these reactions more probable in a given unit of time than they would be in the experiments. However, it is also possible that having excess oxygen on the surface catalyzes reactions that would otherwise not take place. Additional trajectory studies with oxygen concentrations more finely tuned to those likely to exist in the experiments would be beneficial.

When the oxygen-containing ring of Models B and C (those with oxygen coverages closest to what one expects experimentally) underwent a ring opening, 76.5% of the time it resulted in the formation of two additional semiquinones. As will become clear below, it was a semiquinone that was almost always critical to the formation of CO/CO_2. The rate of carbon loss (erosion rate) from our sheets ($\leq$8%) was lower than what has been observed under similar conditions experimentally ($\sim$12.5%).[2] However, if the Models B and C structures that resulted after the first collision were to be exposed to an additional oxygen atom impact, then it is reasonable to expect that their erosion rate might approach or exceed 12.5%. This suggests that an accurate theoretical estimate of the experimental erosion rate might be made by examining collisions with an ensemble of these kinds of structures.

The mechanisms of the more broadly interesting reactions are discussed in detail below.

A. CO Production. The production of CO occurred by way of two different mechanisms. We identified a reaction that resulted in the release of CO from the surface-side of the graphene sheet. This reaction is illustrated in Figure 5a. In it, the incoming oxygen atom struck the oxygen atom in the semiquinone group (panel 2). It vibrationally excited the sheet and formed an epoxide group. The two epoxide groups neighboring the semiquinone group moved atop respective carbon atoms neighboring the semiquinone (panel 3). Bonds then broke sequentially and released the CO, producing two new semiquinone groups (panels 4−6).

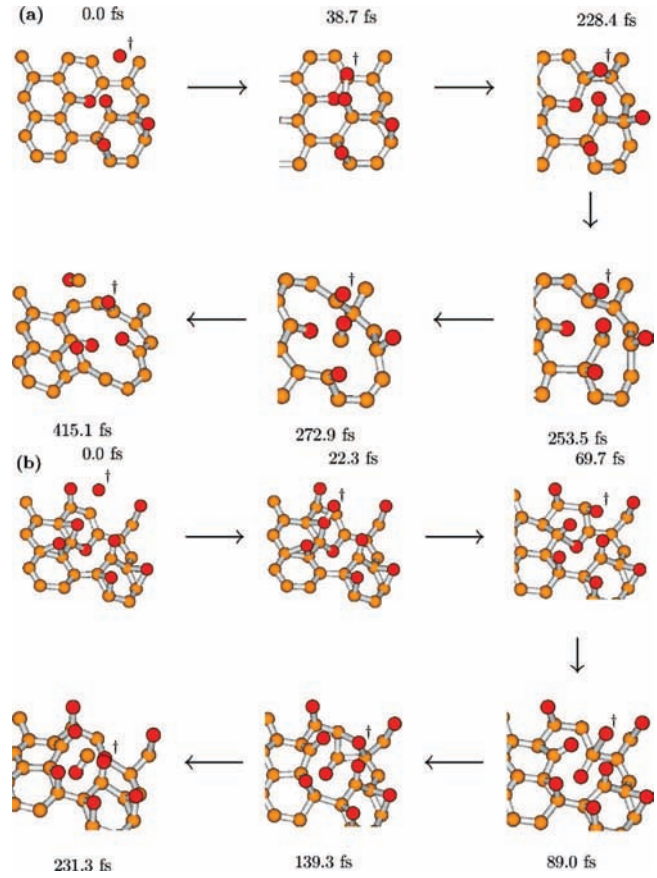

Figure 5. Reactions producing CO. Trajectories resulting in the release of CO from (a) the surface side and (b) the bulk side (b) of the graphene sheet. To help guide the eye, the incoming oxygen atom is labeled with a "†". See the text for descriptions of the details of the trajectories. Note that in some panels only part of the graphene sheet is shown. Also, in many cases, it was rotated. Both were done to provide a better view of the areas involved in and adjacent to the reaction of interest.

The observation of this reaction was not unexpected. As explained in Section I, this type of reaction is thought to play an important role in combustion chemistry.[11,12]

Bulk-side release of CO was also observed. A trajectory in which this took place is illustrated in Figure 5b. In this trajectory, the incoming oxygen atom had an inelastic collision with an epoxide group (panel 2). It then became bonded to a neighboring carbon atom in a structure in which it moves between being in an atop oxygen-like (panel 3) and an epoxide-like (not shown) configuration. Ring opening and epoxide migration resulted in the formation of an sp^3 carbon atom (panel 4). A four-membered ring formed, which included the oxygen atom that was initially incoming (panel 5). It broke, releasing the CO to the bulk side of the sheet (panel 6).

There is some question as to whether this mechanism would be viable for graphite as opposed to graphene. In graphite, there would be a graphene layer $\sim$3.4 Å away from the bulk side of the surface layer. It is not entirely clear if this additional layer would prevent the formation of the transition state that is necessary to form CO or if it would form and subsequently be released after interacting with the subsurface layer. The leading oxygen atom is $\sim$3 Å below the basal plane when the carbon−carbon bond holding the CO is broken (extends beyond 2 Å), so it might be possible. Studies are currently underway to investigate the role of an additional bulk-side graphene layer.

B. CO_2 Production. CO_2 was produced by way of three types of mechanisms. These are illustrated in Figure 6. Figure

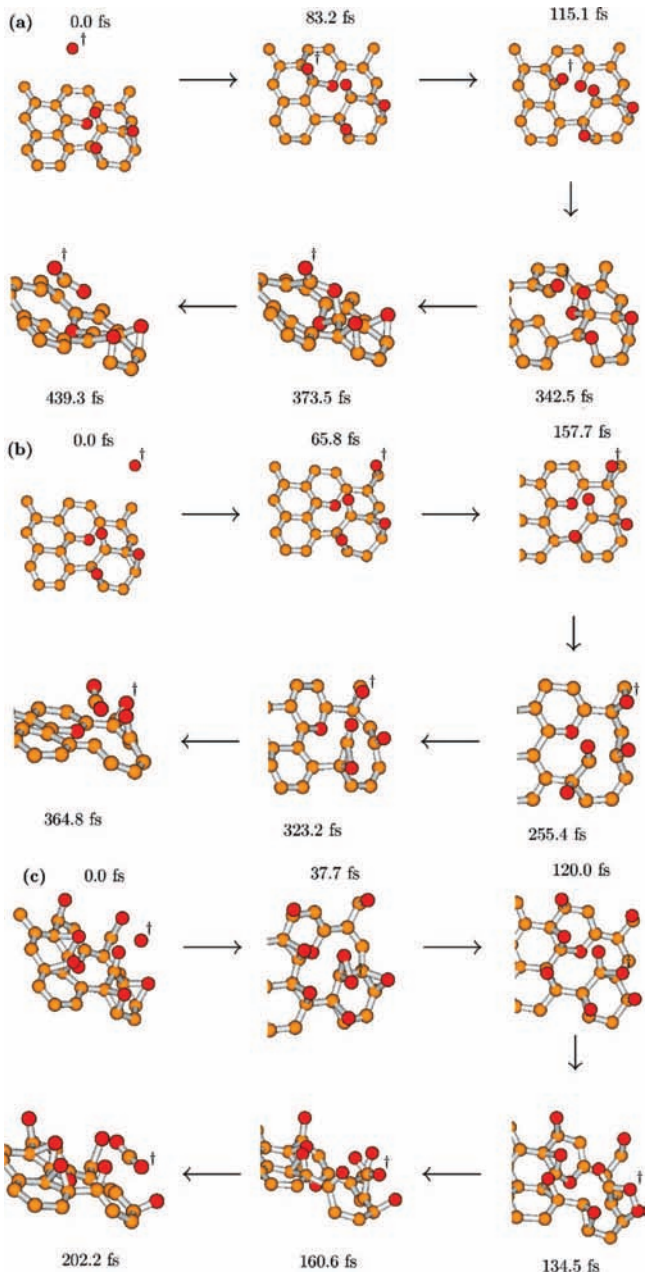

Figure 6. Reactions producing CO_2. (a) A nearly formed CO molecule removed an oxygen atom from a semiquinone group as it receded. (b) A nearly formed CO molecule left a semiquinone group and removed an oxygen atom from a neighboring epoxide group as it receded. (c) Dioxirane formed after a collision with the semiquinone carbon, which then left as CO_2. See the text for a more detailed explanation of these trajectories. The "†" symbols in the fourth panel of a and second and third panels of c are partially obscured by underlying bonds or atoms.

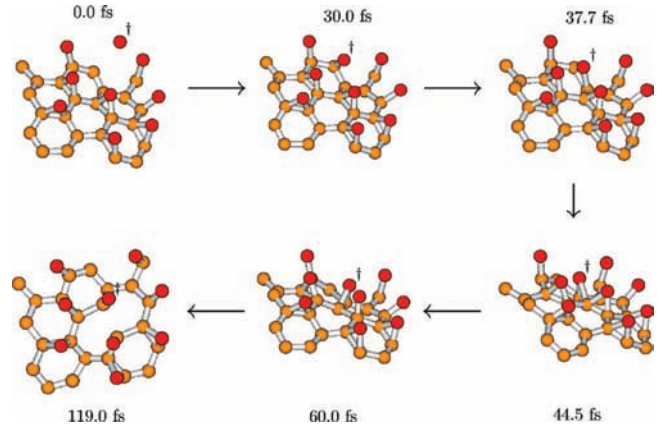

Figure 7. Evidence of damage to a pristine sheet. The collision caused the creation of a pair of semiquinone groups. Note how quickly the events occurred. The "†" symbol in the sixth panel is partially obscured by an underlying bond.

6a shows how the vibrational excitation of a sheet (panels 2 and 3) leads to the opening of the oxygen-containing ring and the formation of a pair of semiquinone groups. Subsequent vibrations lead to the breaking of a carbon−carbon bond and the formation of a new oxygen-containing ring. The formation of the ring changed the hybridization of the precollision semiquinone carbon atom from sp^2 to sp^3. A new carbon−oxygen bond formed (panel 5), and a CO_2 molecule was released (panel 6).

Figure 6b shows a different mechanism, whose early stages are similar to those described in relation to the mechanism for the release of CO, which was illustrated in Figure 5a. In the present case, the impact of the incoming oxygen atom occurred close to the pair of epoxides neighboring the semiquinone. (Note that because of the PBCs, a collision at the top right of the sheet is "near" the atoms at the bottom right of the sheet.) These epoxide oxygen atoms flipped atop respective carbon atoms neighboring the semiquinone group (panel 3). One of the carbon−carbon bonds to the semiquinone broke (panel 4). Rather than leave on its own, the nearly formed CO became bonded to an atop oxygen atom (panel 5) and departed the sheet as a CO_2 molecule (panel 6).

Figure 6c shows a third mechanism by which CO_2 was created. In this case, the incoming oxygen atom struck the semiquinone oxygen and carbon atoms, forming a dioxirane (panel 2). The three-membered ring opened as a bond formed with a neighboring atop oxygen atom, and it broke between two carbon atoms (panels 3 and 4). The CO_2 was then released (panels 5 and 6).

The ground electronic state of CO_2 is a singlet. Consistent with this, in all cases in which CO_2 was produced in the triplet calculations, it was produced in a singlet state (i.e., there was no evidence of any significant spin polarization in the atoms of the CO_2). Instead, the excess spin in the system was spread relatively evenly over all of its atoms.

These three mechanisms as well as the two described in relation to the production of CO are complex. Therefore, they are consistent with the hyperthermal scattering along the surface normal that was observed experimentally. (See Figure 3.) Our simulations are too short to provide insight into the mechanisms responsible for the thermal components of the flux.

C. Damage to a Sheet, Initially without a Hole. We also observed a mechanism that resulted in damage to the pristine sheet. Figure 7 shows one such trajectory. A hard hit between the incoming oxygen and a carbon atom (panel 2) created an epoxide (panel 3), which quickly migrated across the sheet (panels 3 and 4). It collided with another epoxide group (panel 4), causing it to become an atop oxygen atom (panels 4 and 5). Subsequently, a carbon−carbon bond broke, forming two semiquinone groups (panel 6). Note that the reaction quickly proceeded because of the initial low-impact-parameter collision between the incoming oxygen and a carbon atom.

As has already been demonstrated, semiquinone groups can leave the sheets as a result of localized vibrational excitation or after direct collision with incoming oxygen atoms. Therefore, there is every reason to expect that semiquinone groups formed in pristine sheets will lead to the creation of larger holes in the

surface layer of graphite when it is exposed to a continued oxygen-atom flux.

The sheet was exposed to a flux of 1.5×10^{16} oxygen atoms per cm^2. This is a small value compared with those sometimes used experimentally, which can be on the order of 10^{20} oxygen atoms per cm^2.[2] The fact that hole-forming events were observed three and two times in the singlet and triplet trajectories, respectively, suggests a high rate of hole formation in our simulations. Under similar conditions, rough hillock-covered surfaces are observed experimentally.[2] These surfaces are consistent with a high rate of new hole formation.

VI. Conclusions

When HOPG is exposed to a flux of hyperthermal oxygen atoms, the surface becomes functionalized with epoxides to a concentration of between one and two oxygen atoms per six surface carbon atoms. Epoxide formation does not require ISC between the lowest-energy triplet and singlet potential-energy surfaces, as was previously published. Both theory and experiment suggest that incoming oxygen atoms react efficiently with atoms already on the surface to form oxygen molecules by way of an Eley−Rideal (direct reaction) mechanism.

CO and CO_2 were produced in both the experiments and trajectory studies. Experimentally, both thermal and hyperthermal CO and CO_2 were observed. The hyperthermal components had a maximum along the surface normal and exhibit a secondary maximum near 60° for an incident angle of 45°. These data suggest that most is produced by way of a complex reaction mechanism (the former) and some by way of direct reaction (the latter).

Semiquinones can form at defect sites and in functionalized pristine sheets as a result of O atom collisions. In the case of the latter, new defect sites are formed. Semiquinones are important leaving groups and can form CO and CO_2 by way of complex reaction mechanisms when they become vibrationally excited by O atom collisions. Neighboring epoxides groups catalyze these reactions. Carbonyls are also formed, and it is plausible that when they are struck by incoming O atoms, they provide a source of the CO/CO_2 that experiments suggest can also be formed by way of direct reactions.

Acknowledgment. This work was supported by a grant from the Missile Defense Agency under Cooperative Agreement HQ0006-05-2-0001. G.C.S. was supported by AFSOR grant FA9550-07-1-0095.

Supporting Information Available: Summary of additional reactions observed during the trajectories and the presentation and discussion of supplementary theoretical results. This material is available free of charge via the Internet at http://pubs.acs.org.

References and Notes

(1) Kinoshita, H.; Umeno, M.; Tagawa, M.; Ohmae, N. *Surf. Sci.* **1999**, *440*, 49.
(2) Nicholson, K. T.; Minton, T. K.; Sibener, S. J. *Prog. Org. Coat.* **2003**, *47*, 443.
(3) Nicholson, K. T.; Sibener, S. J.; Minton, T. K. *High Perform. Polym.* **2004**, *16*, 197.
(4) Nicholson, K. T.; Minton, T. K.; Sibener, S. J. *J. Phys. Chem. B* **2005**, *109*, 8476.
(5) Wang, T. S. *J. Thermophys. Heat Transfer* **2001**, *15*, 140.
(6) Ringuette, S.; Dubois, C.; Stowe, R. *Propellants, Explos., Pyrotech.* **2001**, *26*, 118.
(7) Viswanath, K.; Brentner, K. S.; GImelshein, S. F.; Levin, D. A. *J. Thermophys. Heat Transfer* **2005**, *19*, 282.
(8) Burt, J. M.; Boyd, L. D. *AIAA J.* **2007**, *45*, 2872.
(9) Paredes, J. I.; Martínez-Alonso, A.; Tasecón, J. M. D. *Langmuir* **2007**, *23*, 8932.
(10) Walker, P. L., Jr.; Rusinko, F., Jr.; Austin, L. G. *Advances in Catalysis*; Academic Press: New York, 1959; Vol. 11.
(11) Chen, N.; Yang, R. T. *J. Phys. Chem. A* **1998**, *102*, 6348.
(12) Montoya, A.; Mondragón, F.; Truong, T. N. *Fuel Process. Techmol.* **2002**, *77*, 125.
(13) Sánchez, A.; Mondragón, F. *J. Phys. Chem. C* **2007**, *111*, 612.
(14) Paci, J. T.; Belytschko, T.; Schatz, G. C. *J. Phys. Chem. C* **2007**, *111*, 18099.
(15) Sorescu, D. C.; Jordan, K. D.; Avouris, P. *J. Phys. Chem. B* **2001**, *105*, 11227.
(16) Janiak, C.; Hoffmann, R.; Sjövall, P.; Kasemo, B. *Langmuir* **1993**, *9*, 3427.
(17) Xu, Y. J.; Li, J. Q. *Chem. Phys. Lett.* **2004**, *400*, 406.
(18) Frankcombe, T. J.; Bhatia, S. K.; Smith, S. C. *Carbon* **2002**, *40*, 2341.
(19) Li, J. L.; Kudin, K. N.; McAllister, M. J.; Prudomme, R. K.; Aksay, I. A.; Car, R. *Phys. Rev. Lett.* **2006**, *96*, 176101.
(20) Cohen, L. K. *J. Chem. Phys.* **1993**, *99*, 9652.
(21) Hahn, J. R. *Carbon* **2005**, *43*, 1506.
(22) Stevens, F.; Kolodny, L. A.; Beebe, T. P., Jr. *J. Phys. Chem. B.* **1998**, *102*, 10799.
(23) Backreedy, R.; Jones, J. M.; Pourkashanian, M.; Williams, A. *Faraday Discuss.* **2001**, *119*, 385.
(24) Bews, I. M.; Hayhurst, A. N.; Richardson, S. M.; Taylor, S. G. *Combust. Flame* **2001**, *124*, 231.
(25) Incze, A.; Pasturel, A.; Chatillon, C. *Surf. Sci.* **2003**, *537*, 55.
(26) Hall, P. J.; Calo, J. M. *Energy Fuels* **1989**, *3*, 370.
(27) Mann, D. J.; Halls, M. D. *J. Chem. Phys.* **2002**, *116*, 9014.
(28) Isborn, C. M.; Li, X.; Tully, J. C. *J. Chem. Phys.* **2007**, *126*, 134307.
(29) Troya, D. Unpublished report, 2002.
(30) Lee, Y. T.; McDonald, J. D.; LeBreton, P. R.; Herschbach, D. R. *Rev. Sci. Instrum.* **1969**, *40*, 1402.
(31) Zhang, J.; Garton, D. J.; Minton, T. K. *J. Chem. Phys.* **2002**, *117*, 6239.
(32) Zhang, J.; Upadhyaya, H. P.; Brunshold, A. L.; Minton, T. K. *J. Phys. Chem. B* **2006**, *110*, 12500.
(33) Caledonia, G. E.; Krech, R. H.; Green, D. B. *AIAA J.* **1987**, *25*, 59.
(34) Garton, D. J.; Minton, T. K.; Maiti, B.; Troya, D.; Schatz, G. C. *J. Chem. Phys.* **2003**, *118*, 1585.
(35) Garton, D. J.; Brunsvold, A. L.; Monton, T. K.; Troya, D.; Maiti, B.; Schatz, G. C. *J. Phys. Chem. A* **2006**, *110*, 1327.
(36) Gibson, K. D.; Sibener, S. J.; Upadhyaya, H. P.; Brunsvold, A. L.; Zhang, J.; Minton, T. K.; Troya, D. *J. Chem. Phys.* **2008**, *128*, 224708.
(37) Mangan, M. A.; Lindsay, B. G.; Stebbings, R. F. *J. Phys. B: At. Mol. Opt. Phys.* **2000**, *33*, 3225.
(38) Tian, C.; Vidal, C. R. *J. Phys. B: At. Mol. Opt. Phys.* **1998**, *21*, 895.
(39) Tian, C.; Vidal, C. R. *J. Chem. Phys.* **1998**, *108*, 927.
(40) Itikawaa, Y. *J. Phys. Chem. Ref. Data* **2002**, *31*, 749.
(41) Straub, H. C.; Lindsay, B. G.; Smith, K. A.; Stebbings, R. F. *J. Chem. Phys.* **1996**, *105*, 4015.
(42) Sánchez-Portal., D.; Ordejón, P.; Artacho, E.; Soler, J. M. *Int. J. Quantum Chem.* **1997**, *65*, 453.
(43) Soler, J. M.; Artacho, E.; Gale, J. D.; García, A.; Junquera, J.; Ordejón, P.; Sánchez-Portal, D. *J. Phys.: Condens. Matter* **2002**, *14*, 2745.
(44) Perdew, J. P.; Burke, K.; Ernzerhof, M. *Phys. Rev. Lett.* **1996**, *77*, 3865.
(45) Frankcombe, T. J.; Smith, S. C. *Carbon* **2004**, *42*, 2921.
(46) Montoya, A.; Mondragón, F.; Truong, T. N. *J. Phys. Chem. A* **2002**, *106*, 4236.
(47) Troya, D.; Schatz, G. C.; Garton, D. J.; Brunsvold, A. L.; Minton, T. K. *J. Chem. Phys.* **2004**, *120*, 731.
(48) Hu, W.; Lendvay, G.; Maiti, B.; Schatz, G. C. *J. Chem. Phys. A* **2008**, *112*, 2093.

JP9000412